Rock and Soil Mechanics

Volume 43 | Issue 6 Article 2

8-1-2022

Three-dimensional seismic stability of inhomogeneous soil slopes using limit analysis method

Yu-nong LI
Key Laboratory of Green Construction and Intelligent Maintenance for Civil Engineering of Hebei Province, Yanshan University, Qinhuangdao, Hebei 066004, China

Chang LIU
Key Laboratory of Green Construction and Intelligent Maintenance for Civil Engineering of Hebei Province, Yanshan University, Qinhuangdao, Hebei 066004, China

Li-wei WANG
Key Laboratory of Green Construction and Intelligent Maintenance for Civil Engineering of Hebei Province, Yanshan University, Qinhuangdao, Hebei 066004, China

Custom Citation
LI Yu-nong, LIU Chang, WANG Li-wei, . Three-dimensional seismic stability of inhomogeneous soil slopes using limit analysis method[J]. Rock and Soil Mechanics, 2022, 43(6): 1493-1502.

Rock and Soil Mechanics 2022 43(6): 1493−1502 ISSN 1000−7598
https: //doi.org/10.16285/j.rsm.2021.6382 rocksoilmech.researchcommons.org/journal

Three-dimensional seismic stability of inhomogeneous soil slopes using limit analysis method

LI Yu-nong[1, 2], LIU Chang[1, 2], WANG Li-wei[1, 2]
1. School of Civil Engineering & Mechanics, Yanshan University, Qinhuangdao, Hebei 066004, China
2. Key Laboratory of Green Construction and Intelligent Maintenance for Civil Engineering of Hebei Province, Yanshan University, Qinhuangdao, Hebei 066004, China

Abstract: Based on the upper bound limit analysis theorem, the three-dimensional seismic stability of inhomogeneous soil slopes is investigated using the pseudo-dynamic approach, and the explicit expression of the factor of safety is obtained by the gravity increase method (GIM). In addition, the genetic algorithm is used for optimization and the results are verified by comparing with other published data. Parametric studies are performed to investigate the effect of relevant parameters on the stability of slopes. The results indicate that for the slope with the given height, the increase of width-to-height ratio and slope angle, and the decrease of internal friction angle and inhomogeneous coefficient will lead to the reduction of factor of safety. The pseudo-static method yields a larger result compared with the pseudo-dynamic method, and the difference between the results of the two approaches increases with the increases of the horizontal seismic coefficient and the effective internal friction angle, but decreases with the increase of the slope angle. The increasing of the soil amplification factor can lead to a significant decrease in the factor of safety of slope, while changes in the period and velocity of the shear wave have little effect on the stability of slopes. The trace of the slip surface is greatly influenced by the horizontal seismic coefficient, but less affected by the inhomogeneous coefficient.

Keywords: inhomogeneous slope; three-dimensional stability; limit analysis; pseudo-dynamic method; seismic effect

1 Introduction

The seismic stability of slope has always been an important research field in geotechnical engineering. In recent years, slope instability, caused by the frequent occurrence of earthquakes, interrupts transportation in light cases and triggers landslides, debris flows, collapse and other disasters in severe cases, which has posed a great threat to the local economic construction and the safety of people's lives. Therefore, it is imperative to study the seismic stability of slopes. Since the three-dimensional slope failure model is difficult to establish, most of the existing studies usually regard the slope stability problem as a two-dimensional plane-strain case[1−3], while the slope failure often presents prominent three-dimensional characteristics due to the restriction of width, and some limitations exist in treating it as a two-dimensional case[4−5]. In addition, due to the long-term accumulation of slope soil layers and the superimposed load on the top of the slope, the soil strength parameters usually show inhomogeneity along the depth direction. Therefore, it is of great theoretical significance and practical value to investigate the stability of three-dimensional inhomogeneous slopes under seismic effects.

Limit analysis method, on the basis of the basic theory of plastic mechanics, is widely used in slope stability analysis because of its rigorous mechanical assumptions and simple solving process[6]. This method has been applied to the seismic stability analysis of three-dimensional slopes in recent years. Michalowski et al.[7] first established a three-dimensional horn-shaped slope failure model, and obtained the critical slope height by the upper bound limit analysis. On this basis, Michalowski et al.[8] simulated the seismic action by the pseudo-static method, analyzed the seismic stability of the three-dimensional slope, and provided the corresponding stability chart. Gao et al.[9] extended the three-dimensional horn failure mechanism from toe failure to face failure and base failure, the conditions for the occurrence of different slope failure patterns were investigated under seismic action by using the pseudo-static assumption and the upper bound theorem. Zhang et al.[10] introduced the seismic force into the calculation model by the pseudo-static method based on the three-dimensional horn failure model, analyzed the energy dissipation of a two-stage slope in the failure process using the upper bound theorem, and derived the analytical solution of the stability coefficient according to the virtual power principle. Based on the upper bound theorem of limit analysis, Nie et al.[11] analyzed the seismic stability of three-dimensional reinforced slopes using the pseudo-static method by considering two reinforcement configurations: uniform reinforcement and triangular

Received: 19 August 2021 Revised: 03 March 2022
This work was supported by the National Natural Science Foundation for Youth Scientists of China (41807295).
First author: LI Yu-nong, female, born in 1981, Ph.D., Associate Professor, research interests: underground foundation engineering, pile-soil interaction, slope engineering. E-mail: yunongli@ysu.edu.cn

reinforcement. Based on the upper bound theorem of limit analysis, Yang et al.[12] investigated the influence of inhomogeneous soil strength on the seismic stability of three-dimensional two-stage slopes. Xu et al.[13] investigated the influences of reinforcement distribution mode, reinforcement strength, slope angle, seismic force, soil inhomogeneity and anisotropy on the slope stability under seismic effect by pseudo-static method for inhomogeneous anisotropic slopes. Li et al.[14] established a three-dimensional horn failure model with cracks based on the upper bound theorem, and discussed the comprehensive impact of cracks, three-dimensional effects and seismic loads on the slope stability considering the seismic effect by the pseudo-static method. However, homogeneous soil is a prerequisite for most of the above studies, and the impact of soil inhomogeneity on slope stability has been ignored. In addition, the pseudo-static method is adopted in the above studies when considering the seismic effect, while the variation of seismic effects in space and time is not taken into consideration.

Therefore, a three-dimensional inhomogeneous horn failure model is established on the basis of previous studies. Based on the limit analysis method, the seismic force is introduced using the pseudo-dynamic method, and the dynamic characteristics of the seismic load are taken into consideration. By calculating the work rate of external force and the work rate of internal dissipation, the explicit expression of factor of safety is derived using the gravity increase method (GIM), and its optimal solution is obtained by a genetic algorithm. In addition, by comparing the calculation results under static and seismic conditions, the effectiveness of the proposed method and optimization program is verified, and factors that may affect the stability of soil slopes are analyzed. The results are helpful for providing some reference for the seismic design of slopes.

2 Three-dimensional horn failure mechanism

The three-dimensional horn-shaped rotational failure mechanism proposed by Michalowski et al.[7] is adopted in this study, which is shown in Fig.1. It consists of a curvilinear cone with apex angle $2\varphi'$, and the upper and lower contours of the failure mechanism on the symmetry plane are two log-spirals $\widehat{A'C'}$ and $\widehat{AC}$, respectively. The slip surface of $\widehat{AC}$ is assumed to pass through the slope toe C. OA' and OA are the initial radii r_0 and r_0', respectively, the initial rotation angle θ_0 is the included angle with the horizontal direction, and the radii of $\widehat{A'C'}$ and $\widehat{AC}$ can be expressed as

$$r' = r_0' e^{-(\theta-\theta_0)\tan\varphi'} \tag{1}$$

$$r = r_0 e^{(\theta-\theta_0)\tan\varphi'} \tag{2}$$

As shown in Fig.1, the three-dimensional horn failure mechanism can be generated by rotating the circular section of increasing radius about the axis of the rotation center O. r_m is the distance from point O to the center of the circular section, R is the radius of the circular section, which can be expressed as

$$r_m = (r + r')/2 \tag{3}$$

$$R = (r - r')/2 \tag{4}$$

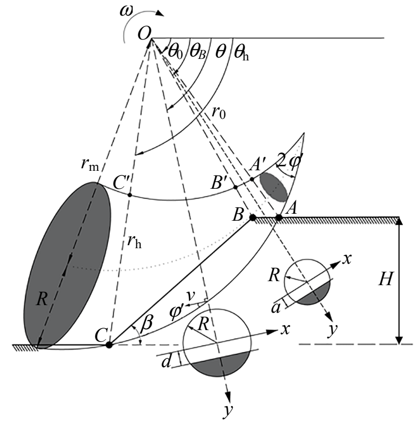

Fig. 1 Three-dimensional failure model with a 'horn-shape' surface

a and d in Fig.1 are the distances from the slope crest AB and the slope face BC to the center line of the curvilinear cone, respectively, θ_B is the included angle between OB and the horizontal line. From the geometric relationship, the above variables can be expressed as

$$a = \frac{\sin\theta_0}{\sin\theta} r_0 - r_m \tag{5}$$

$$d = \frac{\sin(\beta+\theta_h)}{\sin(\beta+\theta)} r_0 e^{(\theta_h-\theta_0)\tan\varphi'} - r_m \tag{6}$$

$$\theta_B = \arctan\frac{r_h\sin\theta_h - H}{H\cot\beta + r_h\cos\theta_h} \tag{7}$$

where β is the slope angle; and r_h is the radius of $\widehat{AC}$ when the rotational angle is θ_h.

When the width-to-height ratio of the soil slope is small, the failure mechanism of the soil slope shows obvious three-dimensional characteristics, and when the width-to-height ratio is large, the slope failure mechanism will gradually change from the three-dimensional mode to the two-dimensional mode. To ensure a smooth transition of the failure mechanism, a sliding block is inserted into the original horn failure mechanism, which can be obtained by stretching the two-dimensional log-spiral failure mechanism by a length of b in the width direction, as shown in Fig.2. The failure mechanism can be approximately regarded as a two-dimensional failure pattern as $b\to\infty$. Suppose that the maximum width of the slope failure area is B after inserting the sliding block, and the maximum width is B' when it is not inserted, therefore,

https://rocksoilmech.researchcommons.org/journal/vol43/iss6/2
DOI: 10.16285/j.rsm.2021.6382

the width b of the plane insert block can be expressed as

$$b = B - B' \tag{8}$$

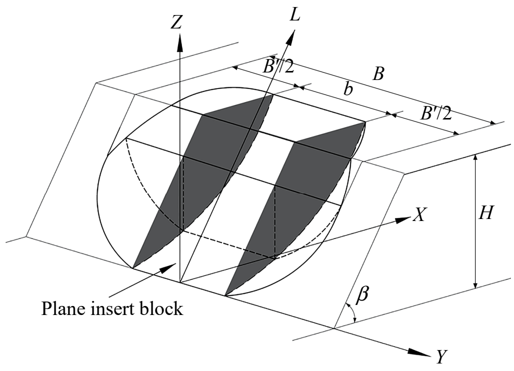

Fig. 2 Schematic diagram of three-dimensional failure model with plane insert block

3 Three-dimensional inhomogeneous soil slope model

The soil inhomogeneity causes great changes in the shear strength of soil, and then affects the stability of the soil slope. It is assumed that the slope soil obeys the Mohr-Coulomb yield criterion, which contains two strength parameters: effective internal friction angle φ' and effective cohesion c'. According to the relevant literature[15–16], it is generally assumed that only c' is inhomogeneous in the depth direction and φ' remains homogeneous.

The three-dimensional inhomogeneous soil slope model[17] is adopted, as shown in Fig.3. It is assumed that the cohesion at the slope toe is c_0, the cohesion at the slope top is n_0c_0 (n_0 is the inhomogeneous coefficient), and the cohesion from the crest to the toe increases linearly with depth, the model can be expressed as

$$c(h) = \left[n_0 + \frac{h}{H}(1 - n_0) \right] c_0 \tag{9}$$

where h is the vertical distance from the crest; H is the height of the slope; and the value of n_0 ranges from 0 to 1. The smaller n_0 is, the stronger the soil inhomogeneity is. The soil can be regarded as homogeneous soil when $n_0 = 1$.

As shown in Fig.3, it can be deduced that the cohesion c_f at the slope face is written as follows according to the geometric relationship.

$$c_f = \left[n_0 + \frac{h_f}{H}(1 - n_0) \right] c_0, \quad \theta_B < \theta < \theta_h \tag{10}$$

where θ_h is the included angle between OC and horizontal direction; and h_f is the vertical distance from the slope face to the crest, which can be expressed as

$$h_f = r_f \sin\theta - r_0 \sin\theta_0 \tag{11}$$

where r_f is the distance from the slope face to point O, which can be expressed as

$$r_f = \frac{\sin(\theta_h + \beta)}{\sin(\theta + \beta)} r_0 e^{(\theta_h - \theta_0)\tan\varphi'} \tag{12}$$

The cohesion c_s at the slip surface can be expressed as

$$c_s = \left[n_0 + \frac{h_s}{H}(1 - n_0) \right] c_0, \quad \theta_0 < \theta < \theta_h \tag{13}$$

where h_s is the distance from the slip surface to the slope crest, which is expressed as:

$$h_s = r_0 e^{(\theta - \theta_0)\tan\varphi'} \sin\theta - r_0 \sin\theta_0 \tag{14}$$

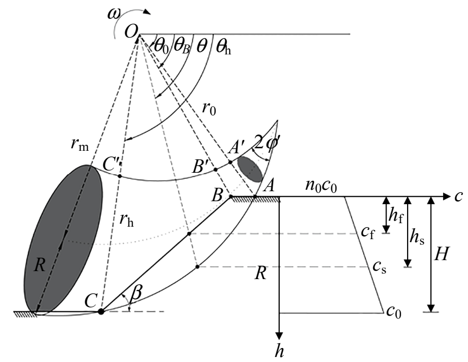

Fig. 3 Three-dimensional inhomogeneous soil slope model

According to the geometric relationship, the cohesion c^{3D} of the three-dimensional horn failure mechanism in the segment from θ_0 to θ_B and segment from θ_B to θ_h are obtained, respectively.

$$c^{3D} = \frac{y - a}{R - a} c_s + \frac{R - y}{R - a} n_0 c_0, \quad \theta_0 < \theta < \theta_B \tag{15}$$

$$c^{3D} = \frac{y - d}{R - d} c_s + \frac{R - y}{R - d} c_f, \quad \theta_B < \theta < \theta_h \tag{16}$$

Substituting Eq.(14) into Eq.(9), the cohesion c^{2D} of the plane insert block can be written as

$$c^{2D} = \left[n_0 + \frac{h_s}{H}(1 - n_0) \right] c_0 \tag{17}$$

4 Work rate of external force and internal energy dissipation

4.1 Upper bound theorem of limit analysis

The upper bound theorem assumes that the slope soil is an ideal elastoplastic material and satisfies the small deformation assumption, and conforms to the associated flow law. The application of the upper bound theorem requires the construction of the kinematically admissible velocity field. Based on the virtual work principle, the upper bound solution of the problem can be obtained by establishing the energy balance equation (the work rate of external force of soil is equal to the work rate of internal dissipation of soil)[15]. The energy balance equation can be expressed as

$$\int_A T_i u_i^* \mathrm{d}A + \int_V F_i u_i^* \mathrm{d}V = \int_V \boldsymbol{\sigma}_{ij} \boldsymbol{\varepsilon}_{ij}^* \mathrm{d}V \tag{18}$$

where T_i and F_i are the surface force and body force of sliding soil, respectively; A and V are the surface area and volume of sliding mass, respectively; $\boldsymbol{\varepsilon}_{ij}^*$ is the strain rate tensor in the kinematically admissible velocity field; $\boldsymbol{\sigma}_{ij}$ is the stress tensor corresponding to the strain rate; and u_i^* is the kinematically admissible velocity field.

4.2 Work rate of external force

The work rate of external force includes both the part W_γ caused by the gravity of the sliding block and the part W_{k_h} caused by the seismic load, and each part consists of a three-dimensional horn failure part and a plane insert block part.

4.2.1 Work rate by soil weight

As shown in Fig.1, the work rate by the soil weight in the three-dimensional horn failure part can be expressed as[7]

$$W_\gamma^{\mathrm{3D}} = 2\gamma\omega\left[\int_{\theta_0}^{\theta_B}\int_a^R\int_0^{\sqrt{R^2-y^2}} (r_\mathrm{m}+y)^2\cos\theta\mathrm{d}y\mathrm{d}x\mathrm{d}\theta + \int_{\theta_B}^{\theta_\mathrm{h}}\int_d^R\int_0^{\sqrt{R^2-y^2}} (r_\mathrm{m}+y)^2\cos\theta\mathrm{d}y\mathrm{d}x\mathrm{d}\theta\right] \tag{19}$$

where γ is the unit weight of soil; ω is the angular velocity of soil rotation. The work rate by the soil weight of the plane insert block can be obtained by multiplying the work rate by the soil weight in the two-dimensional log-spiral mechanism and the width b together, which is expressed as

$$W_\gamma^{\mathrm{2D}} = b\gamma\omega\left[\int_{\theta_0}^{\theta_B}\int_a^R (r_\mathrm{m}+y)^2\cos\theta\mathrm{d}y\mathrm{d}\theta + \int_{\theta_B}^{\theta_\mathrm{h}}\int_d^R (r_\mathrm{m}+y)^2\cos\theta\mathrm{d}y\mathrm{d}\theta\right] \tag{20}$$

Then the total work rate of the soil weight for the failure mechanism is written as

$$W_\gamma = W_\gamma^{\mathrm{2D}} + W_\gamma^{\mathrm{3D}} \tag{21}$$

4.2.2 Work rate by seismic force

In order to reflect the dynamic characteristics of ground motion, the pseudo-dynamic method[18–20] is used to study the seismic stability of three-dimensional soil slopes, where the horizontal and vertical seismic accelerations are simplified as sine functions, and their magnitudes vary with time periodically, which can reflect the cyclic variation of seismic waves with time, so it can truthfully describe the dynamic characteristics of seismic waves. In addition, the pseudo-dynamic method also considers the amplification effect of soil on seismic waves. The amplification effect is expressed by the soil amplification factor f_a, which represents the change of acceleration amplitude from the slope toe to the slope top[21]. Zhang et al.[22] pointed out that the impact of vertical seismic acceleration on slope stability can be ignored when $k_\mathrm{v} \leqslant 0.5k_\mathrm{h}$. Therefore, only the impact of horizontal seismic acceleration is taken into consideration.

The horizontal seismic acceleration a_h in z' away from the slope top at any time t can be expressed as

$$a_\mathrm{h} = k_\mathrm{h} g\left[1+\frac{H-z'}{H}(f_\mathrm{a}-1)\right]\sin\left[2\pi\left(\frac{t}{T}-\frac{H-z'}{\lambda_\mathrm{s}}\right)\right] \tag{22}$$

where k_h is the horizontal seismic coefficient; g is the gravitational acceleration; T is the period of seismic wave; λ_s is the wavelength of seismic wave, $\lambda_\mathrm{s} = TV_\mathrm{s}$, V_s is the speed of the seismic wave in the soil slope; and z' is the vertical distance from any point to the slope top for the failure mechanism, which can be obtained from the geometric relationship as

$$z' = (r_\mathrm{m}+y)\sin\theta - r_0\sin\theta_0 \tag{23}$$

The work rate by the seismic force in the three-dimensional horn failure part can be obtained as follow:

$$W_{k_\mathrm{h}}^{\mathrm{3D}} = \gamma\int_V \frac{a_\mathrm{h}}{g} v\sin\theta\mathrm{d}V \tag{24}$$

where v is the velocity of any point in the sliding block; and $\mathrm{d}V$ is the infinitesimal element volume of any point in the sliding block, which are expressed as

$$v = (r_\mathrm{m}+y)\omega \tag{25}$$

$$\mathrm{d}V = \mathrm{d}x\mathrm{d}y(r_\mathrm{m}+y)\mathrm{d}\theta \tag{26}$$

Substituting Eqs. (22), (23), (25), and (26) into Eq. (24) yields

$$W_{k_\mathrm{h}}^{\mathrm{3D}} = 2k_\mathrm{h}\omega\gamma\left\{\int_{\theta_0}^{\theta_B}\int_a^R\int_0^{\sqrt{R^2-y^2}}(r_\mathrm{m}+y)^2\left[1+\frac{H-z'}{H}(f_\mathrm{a}-1)\right]\cdot \sin\left[2\pi\left(\frac{t}{T}-\frac{H-z'}{\lambda_\mathrm{s}}\right)\right]\sin\theta\mathrm{d}y\mathrm{d}x\mathrm{d}\theta + \int_{\theta_B}^{\theta_\mathrm{h}}\int_d^R\int_0^{\sqrt{R^2-y^2}}(r_\mathrm{m}+y)^2\cdot \left[1+\frac{H-z'}{H}(f_\mathrm{a}-1)\right]\sin\left[2\pi\left(\frac{t}{T}-\frac{H-z'}{\lambda_\mathrm{s}}\right)\right]\sin\theta\mathrm{d}y\mathrm{d}x\mathrm{d}\theta\right\} \tag{27}$$

Similarly, the work rate by the horizontal seismic force in the plane insert block can be derived as follows:

$$W_{k_\mathrm{h}}^{\mathrm{2D}} = bk_\mathrm{h}\gamma\omega\left\{\int_{\theta_0}^{\theta_B}\int_a^R(r_\mathrm{m}+y)^2\left[1+\frac{H-z'}{H}(f_\mathrm{a}-1)\right]\cdot \sin\left[2\pi\left(\frac{t}{T}-\frac{H-z'}{\lambda_\mathrm{s}}\right)\right]\sin\theta\mathrm{d}y\mathrm{d}\theta + \int_{\theta_B}^{\theta_h}\int_d^R(r_\mathrm{m}+y)^2\cdot \left[1+\frac{H-z'}{H}(f_\mathrm{a}-1)\right]\sin\left[2\pi\left(\frac{t}{T}-\frac{H-z'}{\lambda_\mathrm{s}}\right)\right]\sin\theta\mathrm{d}y\mathrm{d}\theta\right\} \tag{28}$$

Then the total work rate by the horizontal seismic force for the failure mechanism is written as:

$$W_{k_{\mathrm{h}}} = W_{k_{\mathrm{h}}}^{\mathrm{2D}} + W_{k_{\mathrm{h}}}^{\mathrm{3D}} \tag{29}$$

4.3 Internal energy dissipation rate

Michalowski et al.[7] pointed out that the internal energy dissipation rate of three-dimensional soil slope instability involves both volume dissipation rate and velocity dissipation rate. The volume dissipation rate is caused by the volume change in the sliding block, and the velocity dissipation rate is the consumed energy that the sliding block overcomes friction along the slip surface. In this paper, the sliding block is assumed to be incompressible, only the velocity dissipation on the slip surface is taken into account, and the influence of volume dissipation is ignored. Therefore, the internal energy dissipation rate for the three-dimensional horn failure part is written as

$$D_{c'}^{\mathrm{3D}} = 2\omega\left[\int_{\theta_0}^{\theta_B}\int_a^R \frac{(r_{\mathrm{m}}+y)^2 R}{\sqrt{R^2-y^2}} c^{\mathrm{3D}} \mathrm{d}y\mathrm{d}\theta + \int_{\theta_B}^{\theta_{\mathrm{h}}}\int_d^R \frac{(r_{\mathrm{m}}+y)^2 R}{\sqrt{R^2-y^2}} c^{\mathrm{3D}} \mathrm{d}y\mathrm{d}\theta\right] \tag{30}$$

The frictional energy dissipation caused by the plane insert block sliding along the slip surface can be expressed as

$$D_{c'}^{\mathrm{2D}} = b\omega\int_{\theta_0}^{\theta_{\mathrm{h}}} c^{\mathrm{2D}} r_0^2 \mathrm{e}^{2(\theta-\theta_0)\tan\varphi'} \mathrm{d}\theta \tag{31}$$

Substituting Eqs. (15) and (16) into Eq. (30) and Eq. (17) into Eq. (31), respectively, it can be deduced as

$$D_{c'}^{\mathrm{3D}} = 2\omega\left[\int_{\theta_0}^{\theta_B}\int_a^R \frac{(r_{\mathrm{m}}+y)^2 R}{\sqrt{R^2-y^2}}\left(\frac{y-a}{R-a}c_{\mathrm{s}} + \frac{R-y}{R-a}n_0 c_0\right)\cdot \mathrm{d}y\mathrm{d}\theta + \int_{\theta_B}^{\theta_{\mathrm{h}}}\int_d^R \frac{(r_{\mathrm{m}}+y)^2 R}{\sqrt{R^2-y^2}}\left(\frac{y-d}{R-d}c_{\mathrm{s}} + \frac{R-y}{R-d}c_{\mathrm{f}}\right)\mathrm{d}y\mathrm{d}\theta\right] \tag{32}$$

$$D_{c'}^{\mathrm{2D}} = b\omega\int_{\theta_0}^{\theta_{\mathrm{h}}}\left[n_0 + \frac{h_{\mathrm{s}}}{H}(1-n_0)\right] c_0 r_0^2 \mathrm{e}^{2(\theta-\theta_0)\tan\varphi'} \mathrm{d}\theta \tag{33}$$

Then the total internal dissipation rate for the failure mechanism is written as

$$D_{c'} = D_{c'}^{\mathrm{3D}} + D_{c'}^{\mathrm{2D}} \tag{34}$$

4.4 Factor of safety and its optimization

The stability of a slope with a given height can be evaluated by the factor of safety F_{s} in geotechnical engineering. The strength reduction method (SRM) and gravity increase method (GIM) are two common methods for calculating the factor of safety F_{s}[23]. SRM has been widely used in slope stability assessment. However, only the implicit expression of F_{s} can be obtained when the limit analysis is applied, which is very time-consuming in the three-dimensional case. On the contrary, an explicit expression of F_{s} can be obtained by the GIM method, which is convenient in engineering applications. Therefore, GIM is used to solve F_{s} in this paper, which can be expressed as the ratio of the dissipation rate to the work rate of external force, that is

$$F_{\mathrm{s}} = \frac{D_{c'}}{W_\gamma + W_{k_{\mathrm{h}}}} \tag{35}$$

F_{s} can be regarded as the function of the optimization variables θ_0, θ_{h}, r_0'/r_0, and t/T, which should meet the following constraints:

$$\left.\begin{aligned} &0 < \theta_0 < \theta_B < \theta_C < \theta_{\mathrm{h}} < \pi \\ &0 < r_0'/r_0 < 1 \\ &0 \leqslant t/T \leqslant 1 \end{aligned}\right\} \tag{36}$$

Therefore, the problem of searching for the minimum factor of safety is transformed into an optimization problem for a multivariable function under constraints, namely:

$$F_{\mathrm{smin}} = \min f(\theta_0, \theta_{\mathrm{h}}, r_0'/r_0, t/T) \tag{37}$$

In this paper, a genetic algorithm is used to optimize the calculation of the factor of safety. Compared with the cyclic search method and the random search method, the genetic algorithm is faster, more accurate, and closer to the global optimal solution. The minimum factor of safety for soil slope with given constraints and the corresponding value of optimization variables can be obtained by using MATLAB software for programming.

5 Comparison and verification

In order to verify the effectiveness of the proposed method and the optimization program, the results of this paper are compared with those in the literature[23−24].

5.1 Comparison under static condition

Literature[24] calculated the stability coefficient $\gamma H/c$ of a three-dimensional homogeneous soil slope under static conditions in the limit state by the limit analysis method. The horizontal seismic coefficient k_{h} and the inhomogeneous coefficient n_0 are set as 0 and 1, respectively, the inhomogeneous slope under seismic conditions is degraded to the homogeneous slope under static conditions for comparison. The corresponding parameters are set as c' = 20 kPa, γ = 20 kN/m^3 in the comparison process, therefore, the critical height H_{cr} of the soil slope in the limit state (F_{s} = 1) can be calculated through the stability coefficient $\gamma H/c$ obtained by the literature[24], and then H_{cr} is substituted into Eq.(35) to obtain the factor of safety F_{s}. Table 1 and Fig.4 illustrate the comparison between the factor of safety and the corresponding critical slip surface obtained by this paper and the literature[24] under different cases. It can be seen that the maximum error between the two results does not exceed 1.1% in the limit state, and the critical slip surface is in good agreement.

Table 1 Comparison between the factors of safety calculated by this study and by the literature[24]

Case	φ' /(°)	β/(°)	B/H	Factor of safety F_s	
				Literature[24]	This study
1	15	90	1.5	(6.783) 1.000	0.989
2	15	90	5.0	(5.456) 1.000	0.997
3	30	90	3.0	(7.632) 1.000	0.999

Note: The figures in brackets refer to the stability coefficients of soil slope by literature [24] in the limit state.

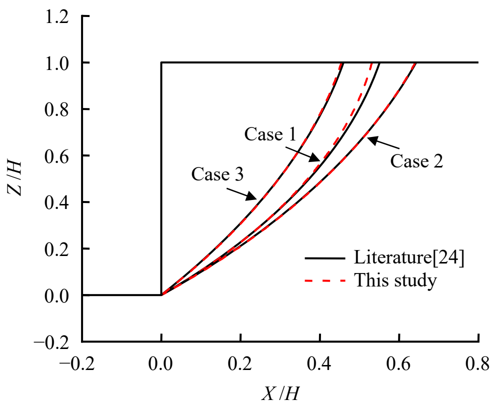

Fig. 4 Comparison of critical slip surface under different working conditions

Figure 5 illustrates the comparison between the factor of safety calculated by the GIM and by the literature[23] as $k_h = 0$. It can be seen that the factors of safety obtained under different width-to-height ratios are very close to that in the literature[23], indicating that the proposed method also has good applicability under static conditions.

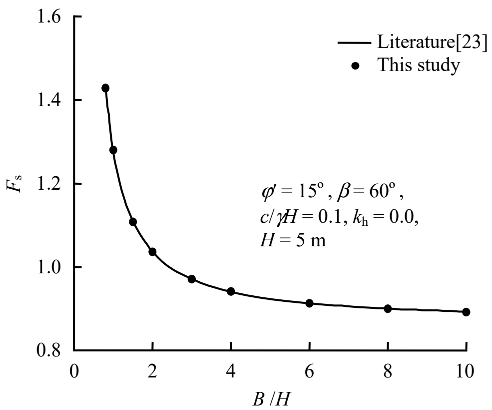

Fig. 5 Comparison between the factor of safety calculated by this paper and that by the literature[23] under static condition

5.2 Comparison under seismic condition

Literature[23] adopts the pseudo-static method to consider the seismic action, and in this paper, by setting the pseudo-dynamic parameter time t to $0.25T$, the soil amplification factor f_a to 1, and the shear wave velocity V_s to infinity, the pseudo-dynamic method is degraded to the pseudo-static method. Meanwhile, the inhomogeneous coefficient n_0 is set as 1, and the inhomogeneous slope is degraded to a homogeneous one. The comparison results are shown in Fig.6, the factor of safety under different k_h are compared respectively, and the corresponding parameter settings are shown in the figure. It can be seen that the results of the two methods are essentially the same. Based on the above comparisons, the accuracy of the proposed method and optimization procedure is well demonstrated.

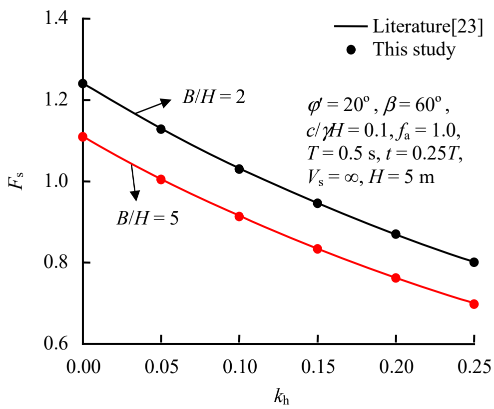

Fig. 6 Comparison between the factor of safety calculated by this paper and by literature [23] under seismic conditions

6 Parameter analysis

6.1 Comparison between the pseudo-dynamic method and the pseudo-static method

The pseudo-static method is widely used in slope engineering currently, but it has great limitations since the dynamic characteristics of seismic force are ignored and the shear modulus and shear wave velocity of soil are assumed to be infinite. In this section, the pseudo-dynamic method is used to obtain the factor of safety under different width-to-height ratio B/H, slope angle β, effective internal friction angle φ', and inhomogeneity coefficient n_0, which is compared with that by the pseudo-static method, the difference between the two methods is discussed to provide a reasonable reference for the seismic stability assessment of slope engineering. The basic calculation parameters are as follows: $H = 5$ m, $\gamma = 20$ kN/m^3, $B/H = 3$, $\varphi' = 20°$, $\beta = 60°$, $n_0 = 1$, $c' = 10$ kPa, $f_a = 1.4$, $T = 0.3$ s, $V_s = 150$ m/s. The corresponding calculation diagram is shown in Fig.7.

DOI: 10.16285/j.rsm.2021.6382

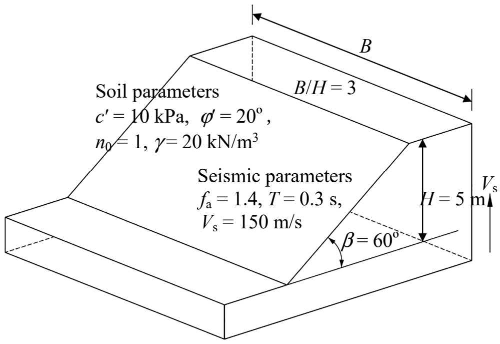

Fig. 7 Calculation diagram

Figure 8 illustrates the comparison between the pseudo-static method and pseudo-dynamic method under different parameters. It can be seen that the slope factor of safety F_s decreases with the increase of horizontal seismic coefficient k_h, indicating that the increase of seismic intensity will significantly reduce the stability of the slope. As shown in Fig.8(a), when the slope height is fixed, F_s increases with the decrease of the width-to-height ratio B/H, indicating that the more obvious the three-dimensional effect of the slope with a certain height (the smaller B/H), the more stable the slope is. The slope can be approximately regarded as a two-dimensional slope when $B/H = 10$. It can be seen that when the three-dimensional effect of the slope is obvious, treating it as a two-dimensional slope will underestimate the stability of the slope. In addition, the sensitivity of the slope with seismic intensity will not vary with B/H. As shown in Fig.8(b), F_s decreases with the increase of slope angle β, indicating that when the slope height is fixed, the slope with larger inclination angel is more likely to be in a critical state. Besides, the sensitivity of slope stability with seismic intensity gradually decreases with the increase of β. As shown in Fig.8(c), a small φ' of the soil slope leads to unfavorable slope stability, and the sensitivity with seismic intensity is also slightly reduced. As shown in Fig.8(d), a small inhomogeneous coefficient n_0 of slope soil corresponds to a small F_s, indicating that the stronger the inhomogeneity of the slope soil, the easier the slope lose stability. In addition, the sensitivity of the slope stability with seismic intensity will not vary with the soil inhomogeneity.

Comparing the curves of the pseudo-static method and the pseudo-dynamic method under different parameters in Fig.8, it can be found that F_s obtained by the pseudo-static method is larger than that by the pseudo-dynamic method, and the difference between the two methods increases with the increase of the horizontal seismic coefficient k_h and the effective internal friction angle φ', while decreases with the increase of β, and remains unchanged with the increase of B/H and n_0. Therefore, when the seismic intensity is small or the slope angle is

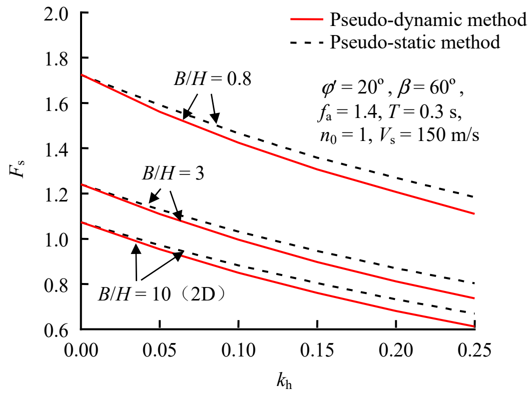

(a) Width-to-height ratio B/H

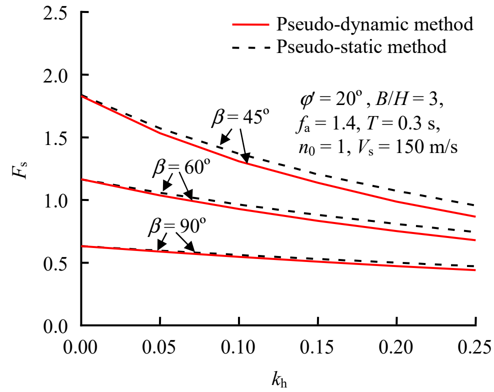

(b) Slope angle β

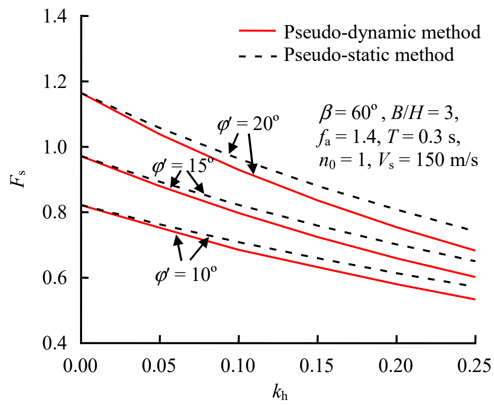

(c) Effective internal friction angle φ'

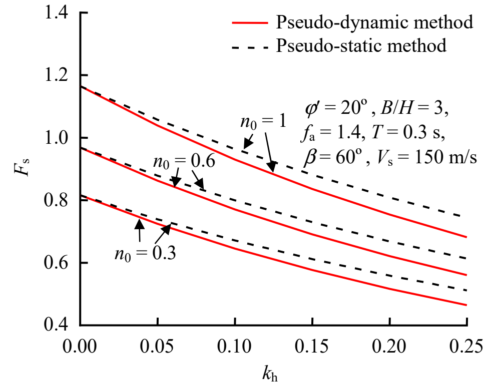

(d) Inhomogeneous coefficient n_0

Fig. 8 Comparison between the pseudo-static and the pseudo-dynamic methods under different parameters

large, it is relatively convenient to use the pseudo-static method in the seismic stability design of slopes. In comparison, the pseudo-dynamic method is undoubtedly the best choice under the premise of ensuring safety and economy.

6.2 Influence of pseudo-dynamic parameters

The influence of pseudo-dynamic parameters (soil amplification factor f_a, seismic wave period T, shear wave velocity V_s) introduced by this method on the slope stability is taken into consideration in this section. The basic parameters are set as: $B/H = 3$, $\beta = 60^\circ$, $\varphi' = 20^\circ$, $c' = 10$ kPa, $n_0 = 0.8$, $f_a = 1.4$, $T = 0.3$ s, $V_s = 150$ m/s.

When the seismic wave transmits from the slope toe to the slope top, the slope soil will amplify the seismic acceleration. The influence of horizontal seismic coefficient k_h on slope factor of safety F_s under different soil amplification factors f_a is shown in Fig.9(a). It can be seen that the increase of soil amplification factor f_a reduces the slope factor of safety F_s significantly under the same seismic intensity, and the decreasing degree becomes more and more evident with the increase of k_h. The reason is that the increase of f_a makes the amplitude of seismic acceleration increase, resulting in the increase of the work rate of external force by the seismic force on the sliding block and further the decrease of the slope factor of safety. Figures 9(b) and 9(c) present the influence of k_h on F_s under different seismic wave periods T and shear wave velocities V_s, respectively. It can be seen that the F_s–k_h curves under different T and V_s are basically in coincidence, indicating that the slope stability is hardly affected by the pseudo- dynamic parameters T and V_s.

Figure 10 illustrates the variation of F_s in a seismic wave period under different k_h and f_a. It can be seen that F_s varies with time t periodically and reaches the minimum value when $t/T \approx 0.32$, and the slope is in the most dangerous state at this time. When f_a is fixed, the increase of k_h will increase the amplitude of F_s significantly, and its value increases with the increase of f_a. For example, the minimum value of F_s decreases from 0.971 to 0.697, a decrease of 28.22%, as $f_a = 1.0$ and k_h increases from 0.1 to 0.3. The minimum value of F_s decreases from 0.935 to 0.624 as $f_a = 1.4$, a decrease of 33.26%. The increase of f_a will also increase the amplitude of F_s when k_h is fixed, and its value will increase with the increase of k_h. For example, f_a increases from 1.0 to 1.4, and F_s increases by 3.71% as $k_h = 0.1$. And F_s increases by 10.47% as $k_h = 0.3$.

6.3 Effect of seismic intensity and soil inhomogeneity on the slip surface

6.3.1 Effect of seismic intensity

Figure 11 shows the top view of the critical slip surface on the symmetrical plane of the three-dimensional soil

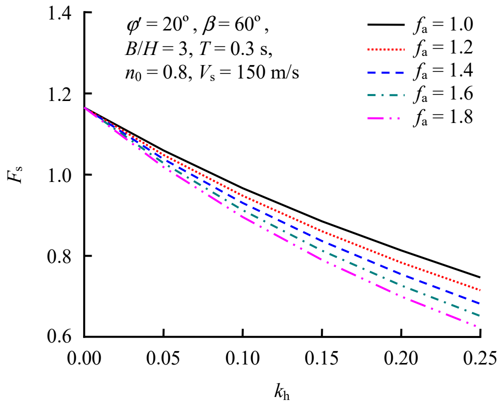

(a) Soil amplification factor f_a

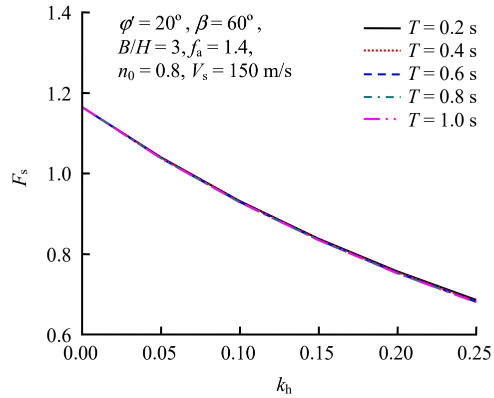

(b) Seismic wave period T

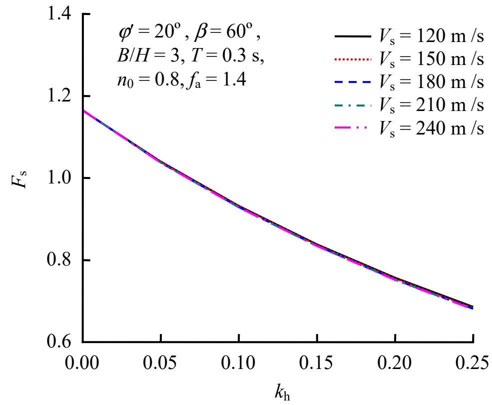

(c) Shear wave velocity V_s

Fig. 9 Influence of different pseudo-dynamic parameters on the factor of safety of soil slope

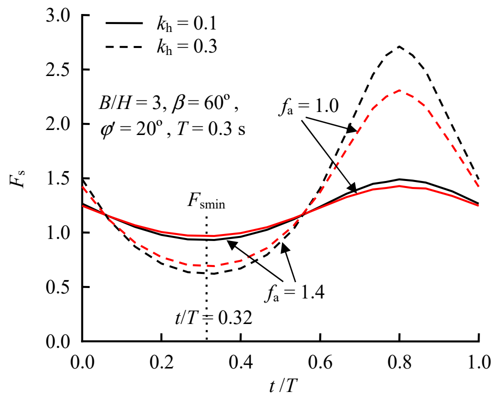

Fig. 10 Variation of the factor of safety of soil slope versus time

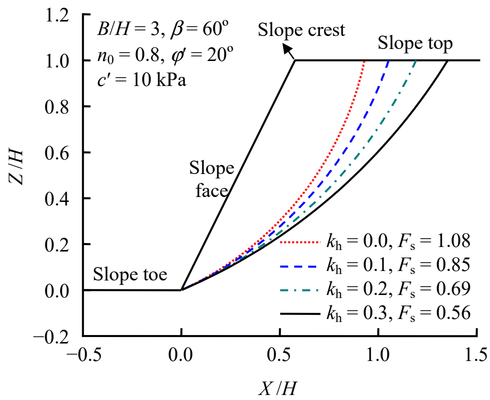

(a) Critical slip surface on the symmetrical plane

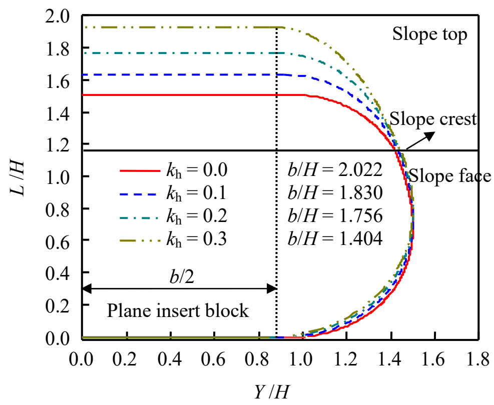

(b) Critical slip surface on slope top and slope face

Fig. 11 Critical slip surface of three-dimension soil slope for different k_h

slope and the trace of the critical slip surface at the slope top and slope face under different seismic intensities. Only half of the slip traces of the whole slope top and slope face are given here because of the symmetry. The relevant parameters are: B/H = 3, β = 60°, φ' = 20°, c' = 10 kPa, n_0 = 0.8, f_a = 1.4, T = 0.3 s, V_s = 150 m/s, respectively. As shown in Fig.11, F_s decreases as the horizontal seismic coefficient k_h increases, the slip surface on the symmetry plane and the slope top is farther away from the slope crest, and the width b of the plane insert block will also gradually decrease, indicating that the increase of seismic intensity decreases the soil slope stability, and the corresponding volume of the sliding block will also increase significantly.

6.3.2 Influence of soil inhomogeneity

Figure 12 shows a top view of the critical slip surface on the symmetrical plane of the three-dimensional soil slope and the trace of the critical slip surface on the top and slope under different inhomogeneous coefficients. The relevant parameters are: B/H = 3, β = 60°, φ' = 20°, c' = 10 kPa, k_h = 0.1, f_a = 1.4, T = 0.3 s, V_s = 150 m/s. As shown in Fig.12, F_s gradually decreases with the decrease of the inhomogeneous coefficient n_0, the slip surface trace of the three-dimensional soil slope on the symmetrical plane slightly moves deeper, the slip surface trace on the top of the slope gradually moves away from the slope crest, while the slip surface trace on the slope face slightly shrinks. In addition, the width b of the plane insert block also gradually decreases, indicating that the stronger the soil inhomogeneity, the worse the stability of the soil slope, while the volume of the sliding body does not change significantly.

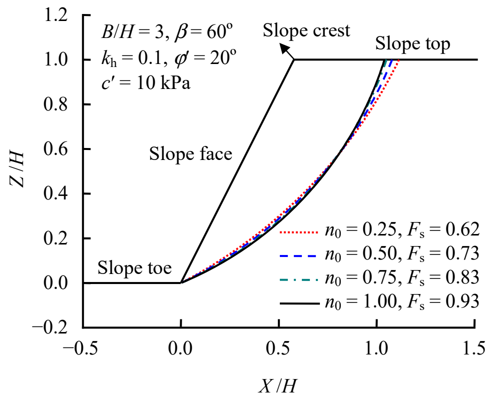

(a) Critical slip surface on the symmetrical plane

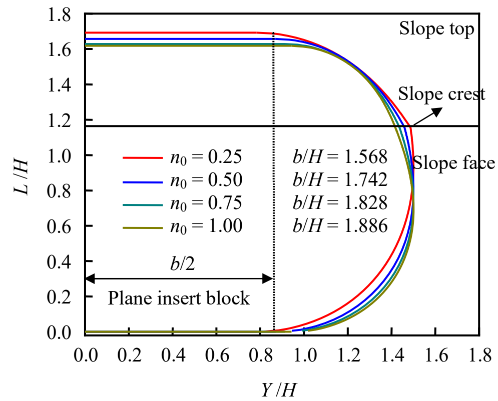

(b) Critical slip surface on slope top and slope face

Fig. 12 Critical slip surface of three-dimension soil slope for different n_0

7 Conclusions

Based on the upper bound theorem of limit analysis, the pseudo-dynamic method is used to study the stability of three-dimensional inhomogeneous soil slope under seismic effect, it is optimized by a genetic algorithm, and the influence of different parameters on the stability of three-dimensional soil slope is analyzed. The main conclusions are as follows:

(1) The increase of k_h leads to a significant decrease of F_s. For the slope with a given height, F_s increases with the increase of φ' and n_0 as k_h is constant, while decreases with the increase of B/H and β. The sensitivity of slope stability with seismic intensity increases with the increase of parameter φ', while decreases with the increase of

parameter β, and remains unchanged with B/H and n_0.

(2) When other parameters are the same, the factor of safety obtained by the pseudo-static method is larger than that by the pseudo-dynamic method, and the difference between the two methods increases with the increase of k_h and φ', while it decreases with the increase of β, and remains unchanged with B/H and n_0.

(3) The decrease of slope stability is caused by the increase of f_a under the same seismic intensity condition, while it is not affected by T and V_s. F_s varies with time t periodically, and the increase of f_a and k_h will increase the amplitude of F_s.

(4) The seismic intensity and soil inhomogeneity will affect the failure trace of the slope. When k_h increases, the slip surface at the symmetry plane and the slope top will be far away from the slope crest, and the volume of the sliding block will also increase significantly. When n_0 decreases, the trace of the slip surface of the slope slightly moves deeper on the symmetrical plane, the slip surface at the slope top is farther away from the slope crest, and the slip surface at the slope face shrinks slightly, while the volume of the sliding block does not change significantly.

References

[1] CHEN Dong, LI Hong-jun, ZHU Kai-bin. Vector sum analysis method for slope stability based on new main sliding trend direction[J]. Rock and Soil Mechanics, 2021, 42(8): 2207−2214.

[2] HE Yi, YU Jun-yan, YUAN Ran, et al. Stability analysis of soil slope with cracks considering upper slope inclination angle[J]. China Journal of Highway and Transport, 2021, 34(5): 45−54.

[3] VAHEDIFARD F, LESHCHINSKY D, MORTEZAEI K, et al. Effective stress-based limit-equilibrium analysis for homogeneous unsaturated slopes[J]. International Journal of Geomechanics, 2016, 16(6): D4016003.

[4] MICHALOWSKI R L, NADUKURU S S. Three-dimensional limit analysis of slopes with pore pressure[J]. Journal of Geotechnical and Geoenvironmental Engineering, 2013, 139(9): 1604−1610.

[5] ZHENG L, LI L, LI J P. Development of three-dimensional failure mechanisms and genetic algorithm for limit analysis of two-layer slopes[J]. Natural Hazards, 2020, 103(3): 3181−3212.

[6] HOU Chao-qun, DENG Xin, SUN Zhi-bin, et al. Upper bound analysis of stability of three-dimensional reinforced slopes based on nonlinear failure criterion[J]. China Journal of Highway and Transport, 2018, 31(2): 124−132.

[7] MICHALOWSKI R L, DRESCHER A. Three-dimensional stability of slopes and excavations[J]. Géotechnique, 2009, 59(10): 839−850.

[8] MICHALOWSKI R L, MARTEL T. Stability charts for 3D failures of steep slopes and excavations[J]. Journal of Geotechnical and Geoenvironmental Engineering, 2011, 137(2): 183−189.

[9] GAO Y F, ZHANG F, LEI G H, et al. Stability charts for 3D failures of homogeneous slopes[J]. Journal of Geotechnical and Geoenvironmental Engineering, 2013, 139(9): 1528−1538.

[10] ZHANG Biao, WANG Xuan, ZHANG Jia-sheng, et al. Three-dimensional seismic stability limit analysis of two-stage slope by kinematical approach[J]. China Journal of Highway and Transport, 2018, 31(2): 86−96.

[11] NIE Xiu-peng, PANG Huan-ping, SUN Zhi-bin, et al. Upper bound analysis of seismic stability of 3D reinforced slopes[J]. Rock and Soil Mechanics, 2019, 40(9): 3483−3492.

[12] YANG X L, XU J S. Three-dimensional stability of two-stage slope in inhomogeneous soils[J]. International Journal of Geomechanics, 2016, 17(7): 06016045.

[13] XU J S, YANG X L. Seismic and static stability analysis for 3D reinforced slope in nonhomogeneous and anisotropic soils[J]. International Journal of Geomechanics, 2018, 18(7): 04018065.

[14] LI Z W, YANG X L, LI T Z. Static and seismic stability assessment of 3D slopes with cracks[J]. Engineering Geology, 2020, 265: 105450.

[15] CHEN W F. Limit analysis and soil plasticity[M]. Amsterdam: Elsevier Science, 1975.

[16] HUANG Mao-song, QIN Hui-lai, GUO Yuan-cheng. Upper bound solution for bearing capacity of nonhomogeneous and anisotropic clay foundation[J]. Chinese Journal of Rock Mechanics and Engineering, 2008, 27(3): 511−518.

[17] LI Jing-pei, GONG Wei-bing, LI Lin, et al. Upper-bound limit analysis on stability of three-dimensional slopes considering soil nonhomogeneity[J]. Journal of Tongji University (Natural Science), 2018, 46(10): 1360−1365.

[18] STEEDMAN R S, ZENG X. The influence of phase on the calculation of pseudo-static earth pressure on a retaining wall[J]. Géotechnique, 1990, 40(1): 103−112.

[19] CHOUDHURY D, NIMBALKAR S. Seismic passive resistance by pseudo-dynamic method[J]. Géotechnique, 55(9): 699−702.

[20] BASHA B M, BADU G L S. Computation of sliding displacements of bridge abutments by pseudo-dynamic method[J]. Soil Dynamics and Earthquake and Engineering, 2009, 29(1): 103−120.

[21] NIE Xiu-peng. Upper limit analysis of three-dimensional reinforced slope stability under complex working conditions[D]. Hefei: Heifei University of Technology, 2020.

[22] ZHANG F, GAO Y F, WU Y X, et al. Effects of vertical seismic acceleration on 3D slope stability[J]. Earthquake Engineering and Engineering Vibration, 2016, 15(3): 487−494.

[23] YANG X L, LI Z W. Comparison of factors of safety using a 3D failure mechanism with kinematic approach[J]. International Journal of Geomechanics, 2018, 18(9): 04018107.

[24] GAO Y F, ZHANG F, LEI G H, et al. An extended limit analysis of three-dimensional slope stability[J]. Geotechnique, 2013, 63(6): 518−524.